BIOCHEMISTRY
including biophysical chemistry & molecular biology
Article

Biochemistry **2010,** *49,* 4227–4234 4227
DOI: 10.1021/bi1001823

A Nonheme High-Spin Ferrous Pool in Mitochondria Isolated from Fermenting *Saccharomyces cerevisiae*[†]

Gregory P. Holmes-Hampton,[‡] Ren Miao,[‡] Jessica Garber Morales,[‡] Yisong Guo,[§] Eckard Münck,[§] and Paul A. Lindahl*[,‡,∥]

[‡]*Department of Chemistry, Texas A&M University, College Station, Texas 77843-3255,* [§]*Department of Chemistry, Carnegie Mellon University, Pittsburgh, Pennsylvania 15213, and* [∥]*Department of Biochemistry and Biophysics, Texas A&M University, College Station, Texas 77843*

Received February 5, 2010; Revised Manuscript Received April 8, 2010

ABSTRACT: Mössbauer spectroscopy was used to detect pools of Fe in mitochondria from fermenting yeast cells, including those consisting of nonheme high-spin (HS) Fe^{II} species, Fe^{III} nanoparticles, and mononuclear HS Fe^{III} species. At issue was whether these species were located within mitochondria or on their exterior. None could be removed by washing mitochondria extensively with ethylene glycol tetraacetic acid or bathophenanthroline sulfonate (BPS), Fe^{II} chelators that do not appear to penetrate mitochondrial membranes. However, when mitochondrial samples were sonicated, BPS coordinated the Fe^{II} species, forming a low-spin Fe^{II} complex. This treatment also diminished the levels of both Fe^{III} species, suggesting that all of these Fe species are encapsulated by mitochondrial membranes and are protected from chelation until membranes are disrupted. 1,10-Phenanthroline is chemically similar to BPS but is membrane soluble; it coordinated nonheme HS Fe^{II} in unsonicated mitochondria. Further, the HS Fe^{III} species and nanoparticles were not reduced by dithionite until the detergent deoxycholate was added to disrupt membranes. There was no correlation between the percentage of nonheme HS Fe^{II} species in mitochondrial samples and the level of contaminating proteins. These results collectively indicate that the observed Fe species are contained within mitochondria. Mössbauer spectra of whole cells were dominated by HS Fe^{III} features; the remainder displayed spectral features typical of isolated mitochondria, suggesting that the Fe in fermenting yeast cells can be coarsely divided into two categories: mitochondrial Fe and (mostly) HS Fe^{III} ions in one or more non-mitochondrial locations.

Iron serves critical roles in cell biology, generally involving catalytic and redox processes. This transition metal is found in many prosthetic groups, including hemes and iron−sulfur clusters. These groups typically serve as enzyme active sites and redox centers. Dysfunction in cellular iron metabolism has been implicated in aging and in the pathogenesis of diseases involving reactive oxygen species (*1*). Clearly, cells need iron, but they must handle it carefully to avoid being damaged by it. Deciphering how cells do this will require a better understanding of iron trafficking in cells.

Mitochondria are traffic "hubs", used to assemble Fe−S clusters and synthesize hemes. In yeast, the Fe^{II} ions that are used as feedstock for these processes are imported into the matrix through the high-affinity inner membrane transporters Mrs3p and Mrs4p (*2*). The ligands coordinating these species have been hypothesized to be nonproteinaceous and to have low molecular weights (*3*). The matrix-localized yeast frataxin homologue protein Yfh1p apparently shuttles these ions to the scaffold protein Isu1p for Fe−S cluster assembly, and perhaps to ferrochelatase for heme biosynthesis (*4*).

Starting with studies by Flatmark and Tangeras (*5*), efforts have been made to characterize the low-molecular weight mononuclear nonheme Fe species in mitochondria. By exposing the organelles to BPS,[1] a strong chelator of mononuclear Fe^{II} ions, they estimated that ∼25% of mitochondrial Fe is present as a chelatable or labile Fe pool.

Recent fluorescence-based studies in mitochondria from rat hepatocytes indicate a far lower concentration of chelatable Fe. Petrat *et al.* (*6*, *7*) incubated cells with fluorescent indicators that accumulate in mitochondria. Fe binding causes fluorescence quenching, so the presence of residual fluorescence in their samples indicated that the binding reaction was limited by the Fe in mitochondria rather than by the indicator. After the subsequent addition of the tight-binding nonfluorescent chelator 1,10-phenanthroline (phen), it penetrated the mitochondria and replaced the Fe-bound indicator, thereby causing fluorescence recovery. The extent of recovery indicated that the concentration of chelatable Fe in rat liver mitochondria was 12−17 μM. The authors estimated that the chelatable Fe pool corresponded to just ∼0.4% of the total Fe in the organelle. They attributed Tangeras' dramatically higher estimate to adventitious Fe generated during the isolation of the organelle.

As explained by Petrat *et al.* (*6*), the fluorescence/chelator-based approach for quantifying Fe complexes in mitochondria within a cell is superior to directly measuring Fe in isolated mitochondria. This is so because cells need not be disrupted for these experiments,

[†]This study was supported by National Institutes of Health Grants GM084266 (P.A.L.), EB-001475 (E.M.), and T32GM008523 (G.P.H.-H. and J.G.-M.) and the Robert A. Welch Foundation (A1170, P.A.L.).

*To whom correspondence should be addressed. Phone: (979) 845-0956. Fax: (979) 845-4719. E-mail: lindahl@chem.tamu.edu.

[1]Abbreviations: LS, low-spin; HS, high-spin; NHHS, nonheme high-spin; BPS, bathophenanthroline sulfonate; EGTA, ethylene glycol bis(2-aminoethyl ether)-*N*,*N*,*N*′,*N*′-tetraacetic acid.

Published on Web 04/21/2010

such that adventitious Fe is not generated. However, this approach is disruptive in another sense; it destroys the Fe complexes of interest as an inherent part of the detection process. Methods that would allow such complexes to be detected without destroying them would have a distinct advantage, as they could facilitate the eventual isolation and characterization of such complexes. Of course, any such method would be useful only if adventitious Fe could be distinguished from Fe that is functionally associated with mitochondria. In this study, we describe the use of Mössbauer spectroscopy to detect three pools of Fe in mitochondria from fermenting yeast cells, including nonheme high-spin (NHHS) Fe^{II} species, magnetically isolated (i.e., noninteracting) mononuclear HS Fe^{III} species, and Fe^{III} nanoparticles. The major objective of this study was to establish whether these Fe-containing species are located within the mitochondria (where they might serve a metabolic role) or on the exterior of the organelle (where they would be simply artifacts of our isolation procedure and counted as adventitiously bound iron). Our results indicate that they are indeed located inside mitochondria.

EXPERIMENTAL PROCEDURES

Cell Growth and Isolation of Mitochondria. Cultures (25 L) of W303-1B cells were grown on Fe-deficient minimal medium supplemented with 40 μM ^{57}Fe (*8*). Cells were harvested at an OD_{600} of 1.0−1.4 and then transferred to a glovebox (~6 °C, ~1 ppm of O_2). Mitochondria were isolated anaerobically as described previously (*8*−*10*), except that cells were treated with ~1000 units of lyticase/g of wet cells for ~50 min. Also, cells were disrupted with 20−25 strokes of the Dounce homogenizer, and a 14.5 to 18.5% Nycodenz gradient was used. In some experiments, the resuspension buffer contained chelators and/or dithionite (final concentration of 10 mM). Samples isolated with buffers that included 1 mM EGTA are termed EGTA-washed mitochondria. Mössbauer spectra were collected and analyzed as described previously (*8*).

Western blots were obtained using specific antibodies for cellular organelles, including mitochondrial porin (Invitrogen), the vacuolar protein carboxypeptidase Y (CPY) (Invitrogen), the cytosolic protein 3-phosphoglycerate kinase (PGK) (Invitrogen), and the endoplasmic reticular protein Kar2 (Santa Cruz Biotechnology). Goat anti-mouse HRP-conjugated secondary antibodies (Invitrogen) were used with all primary antibodies except Kar2, which used goat anti-rabbit HRP-conjugated secondary antibody (Santa Cruz Biotechnology). Thermo Scientific Enhanced Chemiluminescent (ECL) Western Blotting Substrate was then added. Images were obtained (FujiFilm LAS-4000 mini) with a 10 s standard exposure and the chemiluminescence setting. Images were analyzed using MultiGuage version 3.1.

BPS Experiments. In the first and third experiments (Figure 2A,B and Figure S4), cells were treated with buffers containing 1 mM EGTA for the initial steps, including those used to rinse the cells and for incubation with lyticase. The buffer used just prior to homogenization and in all steps thereafter contained 3 mM BPS. Past the step in which mitochondria were collected from the density gradients, all buffers included 10 mM dithionite. The mitochondrial sample was rinsed and packed into a Mössbauer sample holder which was then frozen anaerobically. Spectra were recorded, and the sample was thawed anaerobically and sonicated for 5 × 15 s with a Branson 450 sonifier at a 60% duty load using a two-step microtip. The sample was then refrozen anaerobically, and the Mössbauer spectrum was recorded again. In the second and fourth experiments (Figure 2C,D and Figure S4 of the Supporting Information), mitochondria were collected with EGTA in all buffers. Just prior to being frozen, the sample was treated with buffer containing 3 mM BPS. Dithionite was also included in the fourth fourth experiment, which involved deoxycholate treatment rather than sonication.

Phenanthroline Experiment. EGTA-washed mitochondria were split into two aliquots; one was left untreated, and the other was treated with 3 mM phen (ACROS Organics). After 30 min, both were packed into Mössbauer cups and frozen anaerobically.

Dithionite and Deoxycholate Experiment. A sample of EGTA-washed mitochondria was split equally and treated with dithionite (final concentration of 10 mM). One half was treated with deoxycholate (ACROS Organics) (final concentration of 0.5%). Samples were frozen after incubation in the glovebox for 30 min.

Whole Cells. Cells were grown on minimal medium under constant shaking and harvested at an OD_{600} of 1.0. Cells were collected by centrifugation at 4000*g* and rinsed with unbuffered 100 μM ethylenediaminetetraacetic acid (EDTA). Cells were rinsed twice with water, packed into a Mössbauer sample holder, and frozen. After spectra had been recorded, cells were thawed anaerobically, sonicated as described above, and refrozen.

RESULTS

All samples of mitochondria were anaerobically isolated from fermenting yeast cells. This involved numerous steps in which samples were suspended in buffer, pelleted by centrifugation, and then resuspended in fresh buffer after the supernatant had been discarded. We refer to these steps as washing. Mitochondria were initially washed with buffers that did not include metal chelators. Such preparations exhibited at a low temperature (5 K) and in weak applied magnetic fields (0.05 T) Mössbauer spectra possessing quadrupole doublets typical of nonheme high-spin (NHHS) Fe^{II} species. Such doublets had been observed in spectra of mitochondria isolated from wild-type (WT) respiring (lactate-grown) cells (*9*). The major objective of this study was to establish whether these Fe^{II} ions were located within fermenting mitochondria, where they might serve a metabolic role, or located on the exterior of the organelle, in which case they would probably be artifacts of our isolation procedure.

Throughout these studies, mitochondrial purity was an important consideration. Western blot analysis of our isolated mitochondria indicated an ~30-fold enrichment of the mitochondrial porin relative to the amount present in cell extracts (Figure S1 of the Supporting Information). In fermenting cells, mitochondria occupy ~3% of the cellular volume (*11*), suggesting that our preparations were relatively pure. Western blot analysis indicated some contaminating vacuolar, endoplasmic reticular and cytosolic proteins, which is generally observed (*10*).

Samples were packed by centrifugation into Mössbauer holders (an open delrin cup) to maximize the amount of Fe examined. However, the resulting spectra (Figure 1) had signal-to-noise ratios lower than those readily obtained with Fe-containing proteins or small molecules, due to the low inherent concentration of Fe in mitochondria (700−800 μM Fe overall and typically 200−300 μM ^{57}Fe in samples grown on ^{57}Fe-enriched media). In spectra of mitochondria, the quality was sufficient to recognize some minor species (no less than ~10%), but insufficient to quantify such species to greater than ±5% precision.

Nonheme High-Spin (NHHS) Ferrous Ions in EGTA-Washed Fermenting Mitochondria. Our initial strategy was to remove adventitiously bound NHHS Fe^{II} by including 1 mM

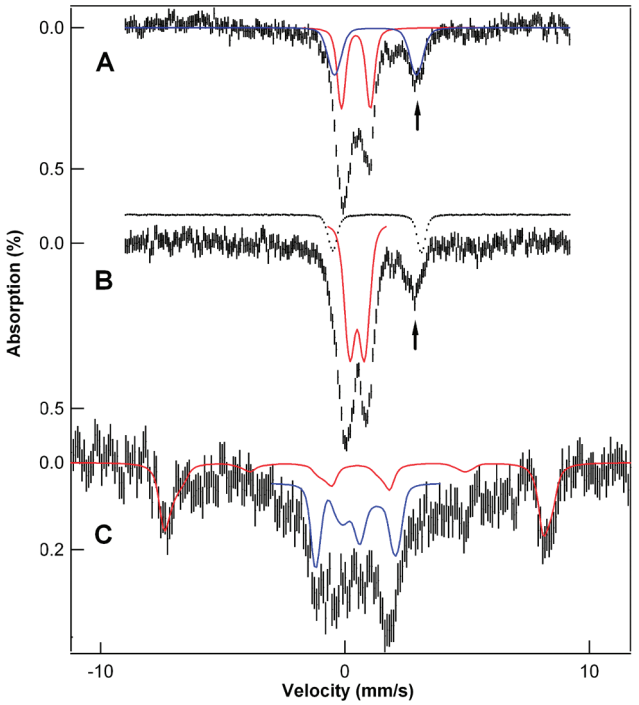

FIGURE 1: Mössbauer spectra of EGTA-washed fermenting mitochondria [sample F12 (*18*)] recorded at 5 K and 0.05 T (A), 100 K and 0.05 T (B), and 4.2 K and 8 T (C). Solid lines simulate the contributions of NHHS Fe^{II} species (blue line in part A, ~20% of total Fe), the central doublet (red line in part A and blue line in part C, ~20% of total Fe), Fe^{III} nanoparticles (red line in part B, ~40% of total Fe), and mononuclear HS Fe^{III} species (red line in part C, ~20% of total Fe). Shown offset above part B is the experimental spectrum of Fe^{II}(EGTA) (black hashmarks). The black arrows in Figures 1−3 point to the high-energy absorption line of the NHHS Fe^{II} species.

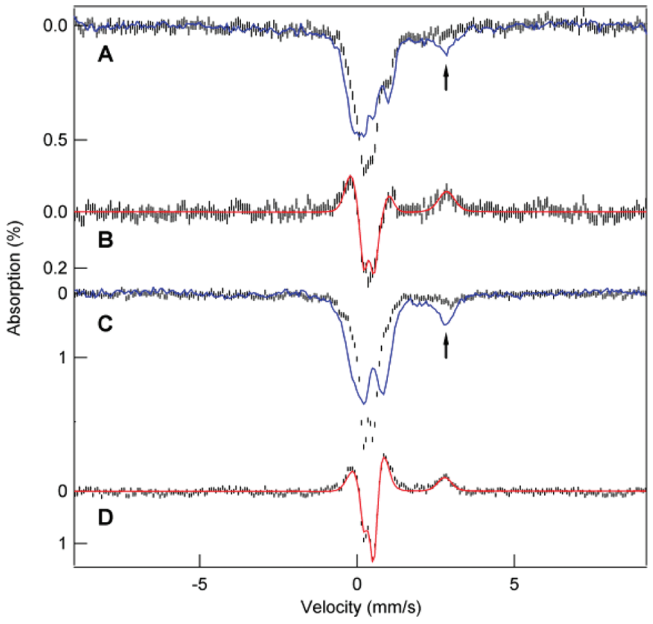

FIGURE 2: Mössbauer spectra (5 K, 0.05 T) of BPS-washed mitochondria [sample F6 (*18*)]. (A) Before (blue line) and after (hashmarks) sonication. (B) After-minus-before difference spectrum. The red line is a simulation assuming that NHHS Fe^{II} (13% of total Fe) and the central doublet Fe (10% of total Fe) were converted into the $Fe^{II}(BPS)_3$ complex (23% of total Fe). Parts C and D are Mössbauer spectra (100 K, 0.05 T) of a second experiment using EGTA-washed mitochondria treated in the final step with BPS [sample F13 (*18*)]. (C) Before (blue line) and after (hashmarks) sonication. (D) After-minus-before difference spectrum. The red line is a simulation assuming that NHHS Fe^{II} (12% of total Fe), Fe of the central doublet (14% of total Fe), and Fe^{III} nanoparticles (34% of total Fe) were converted into $Fe^{II}(BPS)_3$ (60% of total Fe).

EGTA, a strong Fe^{II} chelator, in all washing buffers used during mitochondrial isolation. Such samples were exposed to the chelator for ~6 h overall. In the packing step, all EGTA of the final wash was removed except for that residing between the packed mitochondrial particles [the residual buffer was previously estimated to occupy ~20% of the total volume (*9*, *12*)]. This quantity of residual EGTA was sufficient to coordinate ~200 μM Fe^{II} ions. We chose EGTA because it reportedly does not penetrate mitochondrial membranes (*13*). Also, the Fe^{II}EGTA quadruple doublet can be distinguished reasonably well from the NHHS Fe^{II} doublet associated with our mitochondrial samples. Despite these efforts, the nonheme, non-Fe^{II}(EGTA) HS Fe^{II} doublet was observed in all of the ~30 independently prepared batches of EGTA-washed mitochondria examined. Spectra of four other batches (Figure S2 of the Supporting Information) illustrate the extent of batch-to-batch variation.

The blue line in Figure 1A is a simulation assuming the following isomer shift, quadrupole splitting, and effective line width parameters: $\delta \approx 1.25$ mm/s, $\Delta E_Q \approx 3.35$ mm/s, and $\Gamma = -0.65$ mm/s, respectively (in WMOSS, a negative line width indicates a Voigt profile with a Lorentzian of 0.15 mm/s full width convoluted into a $\sigma = 0.65$ mm/s Gaussian). These values are typical of mononuclear $\{Fe^{2+}(O)_m(N)_n\}$ complexes for which $5 \leq m + n \leq 6$ and $m \geq 4$ (*14*). HS Fe^{II} hemes have δ values ranging from 0.92 to 0.95 mm/s and ΔE_Q values ranging from 2.02 to 2.20 mm/s (*15*, *16*). The low-energy absorption line of the NHHS Fe^{II} doublet is hidden within the central doublet (see below), while the high-energy line, which contains half of the doublet's intensity, is generally resolved. This line is marked by the arrow in Figure 1A and in all other spectra. In Figure 1A, the spectral area of the doublet represents 20% of the Fe in the sample, corresponding to ~150 μM Fe^{II}. The large width of the absorption lines suggests multiple species. This experiment shows that the NHHS Fe^{II} ions in our sample are protected from EGTA chelation despite extensive washing of mitochondria with EGTA-containing buffers.

Mössbauer spectra of fermenting mitochondria also contain a quadrupole doublet representing ~20% of the total Fe (δ = 0.45 mm/s, and $\Delta E_Q \sim 1.15$ mm/s). This species, called the central doublet, arises from unresolved $S = 0$ $[Fe_4S_4]^{2+}$ clusters and low-spin ferrous hemes (Figure 1A, red line) (*8*, *9*). In strong applied fields, the contribution of these species can readily be simulated (Figure 1C, blue line) because the effective field at the nucleus arises solely from the applied field. In contrast, HS Fe^{II} ions exhibit paramagnetic hyperfine structure spread over a wide velocity range, making it difficult to characterize in 8.0 T spectra.

EGTA-washed fermenting mitochondria also exhibited spectral features from magnetically isolated high-spin ($S = {}^5/_2$) mononuclear Fe^{III} species with an E/D value of ~$^1/_3$. In weak applied fields (0.05 T), magnetically isolated Fe^{III} yields intricate Mössbauer patterns exhibiting paramagnetic hyperfine structure. With the low ^{57}Fe concentrations in these samples, such features cannot be analyzed well or easily distinguished from baseline (distorting the quantification of other species). Fortunately, in 8 T applied fields, the outmost features of HS Fe^{III} components are resolved (Figure 1C, red line), allowing an accurate estimate of their concentrations (here 20% of the spectral intensity, corresponding to ~150 μM Fe).

In 0.05 T applied fields, and at 5 K (Figure 1A) and 100 K (Figure 1B), EGTA-washed fermenting mitochondria also yielded a quadrupole doublet with a ΔE_Q of ≈0.63 mm/s and a δ of ≈0.52 mm/s (red line in Figure 1B). Similar doublets were present in spectra of mitochondria isolated from Yfh1p-, Yah1p-, and Atm1p-depleted cells (*4*, *8*, *17*); they arise from Fe^{III} phosphate nanoparticles exhibiting superparamagnetism. In strong applied fields, these nanoparticles yield broad unresolved features (see Figure 2D of ref *8*). Quantification is most accurate at temperatures well above the blocking temperature, T_B; when $T \gg T_B$, spectra consist of a quadrupole doublet (in our samples, $T_B \leq 4.2$ K). The 100 K spectrum (Figure 1B) shows that ~40% of the Fe of the sample belongs to Fe^{III} nanoparticles.

In summary, the Fe in EGTA-washed fermenting WT mitochondria is distributed into four major groups. Approximately 20% is NHHS Fe^{II}, ~20% a combination of $[Fe_4S_4]^{2+}$ and LS Fe^{II} hemes, ~40% Fe^{III} in nanoparticles, and ~20% noninteracting mononuclear high-spin Fe^{III}. These organelles also contain small amounts of other Fe-containing species (*18*). All of these Fe-containing species were present despite extensive exposure of the mitochondria to a strong Fe^{II} chelator, suggesting that they are located within the organelle and protected from chelation.

BPS-Treated Mitochondria. As the difference in the positions of the high-energy lines of the NHHS Fe^{II} doublet and the Fe^{II}EGTA doublet is modest, we wanted more compelling evidence that the NHHS Fe^{II} species in our samples were located within the organelle. BPS is orders of magnitude stronger than EGTA in terms of Fe^{II} chelation, and its negative charge should also make it impenetrable to mitochondrial membranes. However, the major advantage of using BPS is that it forms a LS Fe^{II} complex that can be easily distinguished from HS Fe^{II} ions.

The blue line in Figure 2A is a 5 K Mössbauer spectrum of a mitochondrial sample washed with 3 mM BPS. It contains a NHHS Fe^{II} doublet representing 20% of the total iron. After this spectrum had been recorded, the sample was thawed, sonicated, and refrozen, all in a glovebox containing ~1 ppm O_2. The resulting spectrum (Figure 2A, hash marks) lacked the NHHS Fe^{II} doublet; rather, it exhibited a doublet with a ΔE_Q of 0.32 mm/s and a δ of 0.38 mm/s, indicating LS $Fe^{II}(BPS)_3$. These changes are best visualized by the after-minus-before sonication difference spectrum shown in Figure 2B. Features pointing upward (downward) are present before (after) sonication; unchanged features offset. The spectral simulation (red line) assumes that 23% of the Fe in the sample was converted to $Fe^{II}(BPS)_3$ by sonication, including NHHS Fe^{II} (13%) and the central doublet (10%) (the percentage in parentheses refers to total Fe, not the percent change of the spectral species). The change corresponds to the majority of the initial NHHS Fe^{II} species and to approximately half of the central doublet. Other experiments suggest that sonication alone can destroy $[Fe_4S_4]^{2+}$ clusters (Figure S3 of the Supporting Information), whereas BPS does not chelate Fe^{II} coordinated in heme centers (*19*). We suspect that sonication degraded a large portion of mitochondrial $[Fe_4S_4]$ clusters and that the released Fe ions were reduced by endogenous agents present in mitochondria (or generated upon sonication) to Fe^{II} and coordinated by BPS.

Similar results were observed in a second independent experiment (Figure 2C,D) in which BPS was added to EGTA-washed mitochondria only in the final isolation step. Again, the majority of NHHS Fe^{II} ions and half of the central doublet were replaced by $Fe^{II}(BPS)_3$ after sonication. In this experiment, the majority of the iron contained in the Fe^{III} nanoparticles was also converted to $Fe^{II}(BPS)_3$ upon sonication (the first experiment showed a lower percentage of nanoparticles). We suspect that sonication released species (sulfide ions?) that reduced the Fe^{III} ions of the nanoparticles to HS Fe^{II} ions that were then coordinated by BPS. A third independent experiment (Figure S4 of the Supporting Information) using BPS-washed mitochondria also showed the semiquantitative conversion of NHHS Fe^{II} ions into LS $Fe^{II}(BPS)_3$ upon sonication. Other Fe-containing species in the mitochondria also converted to $Fe^{II}(BPS)_3$, but our spectra are insufficiently resolved for their identification. A fourth experiment was conducted in which membranes were disrupted by being exposed to deoxycholate rather than by sonication. This detergent has been used to disrupt mitochondrial membranes (*22*). The spectra, also shown in Figure S4 of the Supporting Information, again show the presence of NHHS Fe^{II} in the BPS-washed sample, and the replacement of this doublet by the $Fe^{II}(BPS)_3$ doublet in the spectra of the sample treated with deoxycholate. The results of these four experiments establish that the NHHS Fe^{II} ions in our samples were protected from BPS chelation prior to sonication, and that they became susceptible to chelation after sonication. We conclude that this protection arose because these ions are encapsulated by the mitochondrial membrane across which BPS cannot penetrate. Sonication (or deoxycholate) disrupts these membranes, rendering the NHHS Fe^{II} ions accessible to chelation. Depending on the extent of BPS exposure, a portion of the Fe in $[Fe_4S_4]^{2+}$ clusters and/or Fe^{III} nanoparticles can also be chelated by BPS.

Mitochondria Treated with Phenanthroline. From the perspective of Fe coordination, phen and BPS have the same structure and properties; both are extremely strong bidentate chelators that bind HS Fe^{II} to form LS Fe^{II} complexes. However, in contrast to negatively charged BPS, phen is neutral and able to penetrate the mitochondrial inner membrane (IM) (*6*). Thus, if the NHHS Fe^{II} species are inside mitochondrial membranes, phen should chelate these ions in unsonicated mitochondria. To test this, an EGTA-washed mitochondrial sample was divided in two; half was frozen without treatment, and the other half was treated with phen and then frozen. The untreated control (Figure 3A, blue line) is that of Figure 1; it exhibited a HS Fe^{II} doublet representing 20% of the Fe in the sample. The matched phen-treated sample (Figure 3A, black hash marks) lacked the NHHS Fe^{II} doublet but contained an intense quadrupole doublet with a ΔE_Q of 0.31 mm/s and a δ of 0.37 mm/s. These parameters are characteristic of LS $Fe^{II}(phen)_3$. This doublet represented 25% of the total Fe in the sample. These changes are illustrated in the "after-minus-before" difference spectrum (Figure 3B). The red line is a simulation showing 15% NHHS Fe^{II} ions (the features pointing upward) converting to $Fe^{II}(phen)_3$ after being exposed to phen. Some additional Fe species, representing ~10% of the total Fe, also converted to $Fe^{II}(phen)_3$. These species exhibit the upward feature at ~1.2 mm/s in Figure 3B. They might be Fe^{III} nanoparticles or Fe of the central doublet, but the spectra lack sufficient resolution to distinguish them. Phen did not cause the decline of the mononuclear HS Fe^{III} species, perhaps due to the weaker coordination of phen to ferric ions. Regardless, our main conclusion is that phen penetrates unsonicated mitochondria and coordinates the NHHS Fe^{II} ions located therein.

No Correlation of NHHS Fe^{II} to Contamination Levels. One difficulty in determining the cellular location of the observed NHHS Fe^{II} species has been to exclude the possibility that they are encapsulated by membranes other than those of mitochondria.

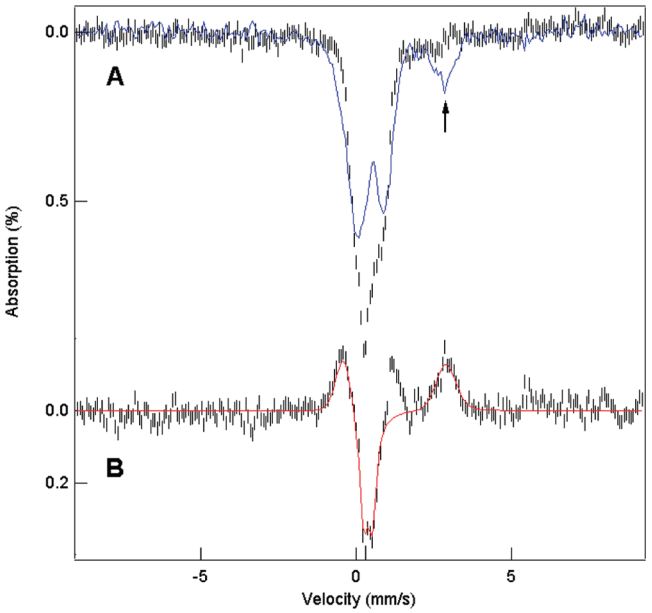

FIGURE 3: Mössbauer spectra (5 K, 0.05 T) of EGTA-washed mitochondria [sample F14 (*18*)] incubated with phen (A, black hash marks) and not incubated (A, blue line). (B) Incubated-minus-not-incubated difference spectrum. The red line is a simulation assuming that NHHS Fe^{II} ions (15% of total Fe) converted to $Fe^{II}(phen)_3$ after being exposed to phen. The remaining $Fe^{II}(phen)_3$ doublet (~10% of total Fe) originated from either Fe^{III} nanoparticles, mononuclear Fe^{III} ions, or irons of the central doublet.

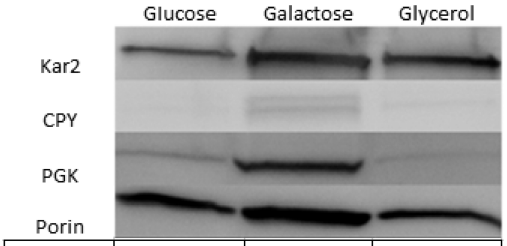

Kar2/Porin	0.57	0.73	1.06
CPY/Porin	0.042	0.15	0.045
PGK/Porin	0.18	0.51	0.2
%NHHS	16%	7%	3%

FIGURE 4: Western blot of extracts of mitochondria from cells grown on glucose (left), galactose (middle), and glycerol (right) [samples F5, RF1, and R1, respectively (*18*)]. For each sample, 60 μg of protein, determined by the bicinchoninic acid method (Thermo Scientific), was added to each lane of a 10% SDS−PAGE gel. Primary antibodies used in staining included Kar2p, CPY, PGK, and porin. Integrated intensities of contaminating bands were normalized to the intensity of the corresponding porin band. These ratios are given in the table along with the percentage of the NHHS Fe^{II} doublet observed in the Mössbauer spectrum of the same material.

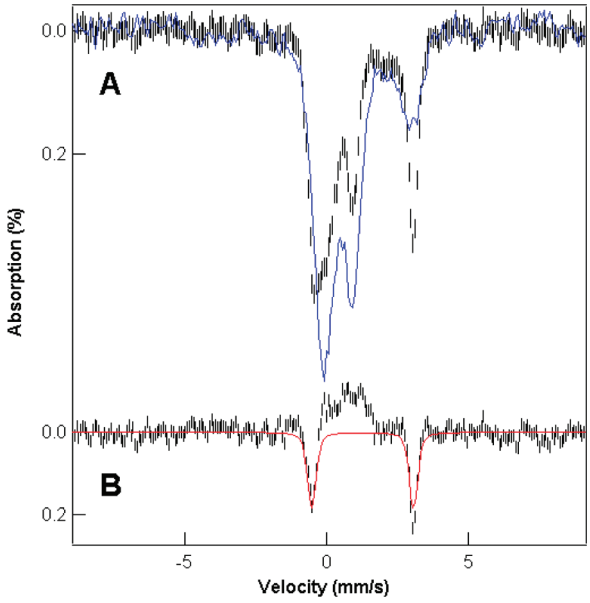

FIGURE 5: Effect of deoxycholate on the ability of dithionite to reduce Fe^{III} species in EGTA-treated mitochondria [sample F15 (*18*)]. (A) Mössbauer spectra (100 K) of EGTA-washed, dithionite-treated, mitochondria in the absence (blue) and presence (black hashmarks) of deoxycholate. (B) Presence-minus-absence difference spectrum of deoxycholate. The red line is a simulation representing 20% of the total Fe with a δ of 1.3 mm/s and a ΔE_Q of 3.6 mm/s.

As discussed previously (*10*, *20*), the best method available for isolating large quantities of mitochondria (i.e., discontinuous density gradient centrifugation) does not remove all non-mitochondrial membranous material; the most common contaminants include endoplasmic reticulum (ER) and vacuoles (*10*). Besides having a density similar to that of mitochondria, the ER physically interacts with mitochondria for phospholipid biosynthesis and calcium signaling (*21*). These interactions might prevent the clean separation of the two organelles.

We have discovered that the percentage of NHHS Fe^{II} differs in mitochondria isolated from cells grown on different carbon sources (*18*). In mitochondrial preparations isolated from cells grown on glucose, galactose, and glycerol, the NHHS Fe^{II} doublet quantified to 16, 7, and 3% of the total Fe, respectively. Western blot analysis confirmed that these preparations contained some contaminating ER and vacuolar proteins (Figure 4). The density of blots obtained using antibodies that bind to proteins in the ER, vacuoles, and cytosol was normalized using antibodies for the porin protein that localizes to mitochondria. We found that the normalized blot densities for contaminating organelles were not correlated to the percentage of the NHHS Fe^{II} doublet (Figure 4, table). Similar analyses performed on eight different batches of mitochondria isolated from glucose-grown cells also showed no correlation (Figure S5 of the Supporting Information). These results indicate that the NHHS Fe^{II} ions present in chelator-washed mitochondria are contained within these organelles rather than in contaminating membranous species such as ER or vacuoles.

Dithionite- and Deoxycholate-Treated Mitochondria. We also used deoxycholate in the presence of the reductant dithionite to evaluate whether the HS Fe^{III} species in our mitochondrial samples were contained within the organelle. We treated half of a WT EGTA-washed fermenting mitochondrial sample with dithionite; the other half was treated with dithionite and deoxycholate.

The low-field spectrum of the dithionite- and deoxycholate-treated sample (Figure 5A, black hashmarks) contained a doublet due to Fe^{II}EGTA with a δ of 1.3 mm/s and a ΔE_Q of 3.6 mm/s (Figure 5A, blue line) that represented 40% of the total Fe. The corresponding spectrum of the dithionite-treated sample exhibited a NHHS Fe^{II} doublet with approximately half that intensity (Figure 5A, blue line). The deoxycholate-treated-minus-untreated difference spectrum (Figure 5B) revealed that besides EGTA coordination to the 20% of the NHHS Fe^{II} species originally in the dithionite-treated sample, ~20% of the Fe from other species was also converted to Fe^{II}(EGTA). High-field spectra (Figure S6 of

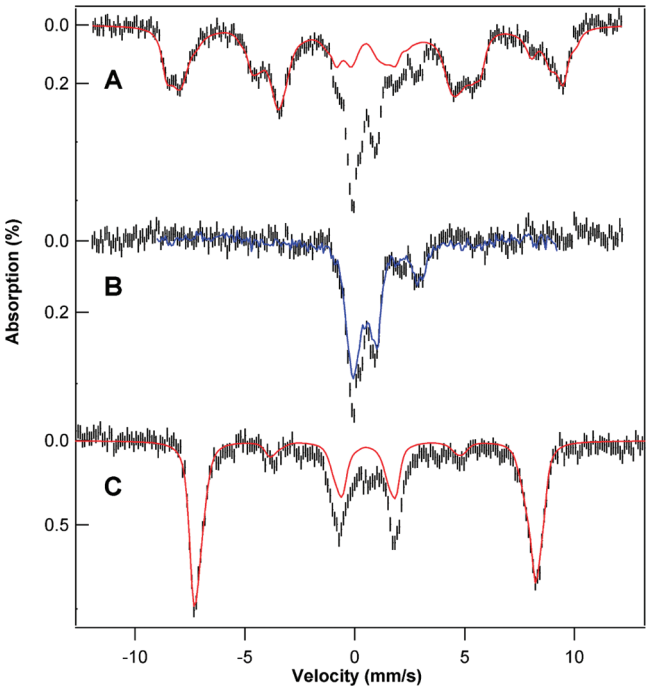

FIGURE 6: Mössbauer spectra (5 K) of whole fermenting yeast cells grown on ^{57}Fe-enriched minimal medium. (A) Applied field of 0.05 T. The red line is a simulation with A values ranging from −21 to −23.5 T. (B) Spectrum obtained after subtraction of the simulation in part A from the data. The blue line is the spectrum of isolated mitochondria given in Figure 1A. (C) Same as part A, but at an applied field of 8.0 T. The red line is a simulation with A values ranging from −21.5 to −22.5 T.

the Supporting Information) reveal that some (~12% of total Fe) of these other species originated from HS mononuclear Fe^{III} species. Spectral features from such species are evident in the 8.0 T spectrum of the dithionite-treated sample but absent in that of the dithionite- and deoxycholate-treated sample. The other iron species contributing to the Fe^{II}(EGTA) complex (~8% of total Fe) could not be identified, but they could be Fe^{III} nanoparticles. The central doublet contribution was unchanged in the experiment, consistent with deoxycholate treatment being gentler than sonication in the disruption of membranes but not damaging Fe_4S_4 clusters. These results suggest that the mononuclear HS Fe^{III} species (and perhaps Fe^{III} nanoparticles) that contribute to the spectra of isolated fermenting mitochondria are contained within these organelles, protected from reduction by dithionite. Disruption of these membranes by deoxycholate removed this protection, allowing dithionite to reduce Fe^{III} to Fe^{II}. EGTA then chelated the Fe^{II} ions forming the observed Fe^{II}(EGTA) doublet.

Whole Yeast Cells. ^{57}Fe-enriched whole fermenting yeast cells exhibited 5 K Mössbauer spectra dominated by features indicating magnetically noninteracting mononuclear HS Fe^{III} components (Figure 6). These components have vanishingly small spin-dipolar interactions with other paramagnetic Fe sites. At 0.05 T (Figure 6A), they display paramagnetic hyperfine structure (a quadrupole doublet would be expected if spin-dipolar interactions were effective or if the Fe^{III} component belonged to nanoparticles with a T_B of $\ll$4 K). At 8.0 T (Figure 6C), such species exhibited patterns characteristic of magnetically noninteracting Fe^{III}. This behavior implies that these components should be EPR active.

The red lines in Figure 6 are the sums of simulations for three mononuclear HS Fe^{III} species, collectively representing ~75% of the spectral intensity; the actual number of species contributing to these features remains undetermined. Individual differences among the HS Fe^{III} species are lost at 8.0 T. The difference spectrum (Figure 6B) obtained by subtraction of the low-field simulation of Figure 6A from the spectrum of Figure 6A is similar to that obtained for isolated mitochondria (the blue line in Figure 6B is the spectrum of EGTA-washed mitochondria shown in Figure 1A).

A detailed analysis of the iron content of entire yeast cells will require a separate analysis, but our current analysis is sufficient for us to draw two major conclusions. First, the magnetically noninteracting mononuclear HS Fe^{III} species (whose contribution was removed from the spectrum of Figure 6A) are not located in mitochondria. Second, the majority of Fe in fermenting yeast cells can be divided into two major groups: these non-mitochondrial mononuclear Fe^{III} species and mitochondrial Fe species.

The non-mitochondrial Fe^{III} species are reduced to the Fe^{II} state upon sonication of cells and treatment with dithionite (Figure S7 of the Supporting Information). The resulting quadrupole doublet had a ΔE_Q of 3.10 mm/s and a δ of 1.35 mm/s, parameters similar to those of the NHHS Fe^{II} doublet in isolated mitochondria. This does not necessarily mean that the two doublets represent the same pool of iron, but this possibility cannot be excluded.

DISCUSSION

NHHS Fe^{II} Pool within Isolated Mitochondria. The major conclusion of this study is that the NHHS Fe^{II} species that are present in our isolated mitochondrial samples are located within the organelle. Three lines of evidence support this. First, such species were observed after intact mitochondria were exposed to high concentrations of strong Fe^{II} chelators (EGTA and BPS) for extensive periods of time. EGTA is reported not to penetrate mitochondrial membranes, and BPS is unlikely to do so because of its negative charge. We have observed such species in all ~30 batches prepared in this way over the course of the past 5 years. These Fe^{II} species were present in samples that had not been sonicated or exposed to phen, indicating that they were not generated by the degradation of [Fe_4S_4] clusters.

Second, BPS and EGTA were able to coordinate NHHS Fe^{II} only after samples had been sonicated. As sonication disrupts mitochondrial membranes, we conclude that the NHHS Fe^{II} species are located within the mitochondria and are protected from these chelators until the mitochondrial membranes are disrupted by sonication or by detergents such as deoxycholate. This conclusion is supported by the observation that phen (with a coordinating chemical structure similar to that of BPS but neutral and membrane permeable) can chelate the NHHS Fe^{II} species without sonication.

Third, there was no correlation between the spectral intensity of the NHHS Fe^{II} doublet and the level of ER or vacuolar contamination in our samples. This excludes the possibility that these Fe^{II} species are located in a membrane-bound but non-mitochondrial organelle that contaminated our preparations.

Other scenarios have also been considered. For example, it is conceivable that during isolation, mitochondrial membranes become more permeable, allowing Fe from the isolation buffers to enter into the organelle. However, in this case, one would also expect that the strong chelators present in these buffers would have also entered the organelle and coordinated the observed HS Fe^{II} species, and/or that Fe within the organelle would also have

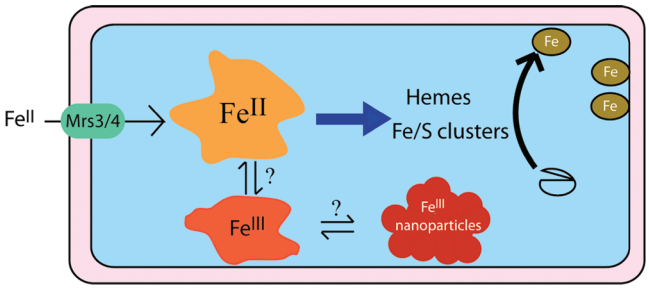

FIGURE 7: Distribution of iron pools in mitochondria isolated from fermenting yeast. Three pools composed of nonheme HS Fe^{II} species, mononuclear HS Fe^{III} species, and Fe^{III} nanoparticles have been identified.

diffused into the buffer, draining the organelle of the observed HS Fe^{II}. The presence of the HS Fe^{II} species argues against these scenarios.

These Fe^{II} components represent ~20% of the total Fe in the organelle (700−800 μM), corresponding to ~150 μM in NHHS Fe^{II}. Given the low intensity of our signals and batch-to-batch variations, we estimate an overall relative uncertainty of ±30% (100−200 μM) for the concentration of these components in fermenting mitochondria. This concentration is 1 order of magnitude higher than previous estimates based on fluorescence studies. Comparing results is difficult because the sources of the mitochondria (yeast vs rat liver) differed as did the metabolic conditions under which the cells were prepared. Nevertheless, our studies show that the concentration of these ions in mitochondria isolated from fermenting yeast is higher than what has been generally assumed.

Other Pools of Iron in Mitochondria and Whole Cells. Although the focus of this paper was to establish whether the NHHS Fe^{II} species were located within yeast mitochondria, our experiments also provide evidence of other pools of Fe in the organelle, including Fe^{III} nanoparticles (~40% of the Fe, corresponding to ~300 μM, but somewhat variable) and mononuclear HS Fe^{III} ions (~20% of the Fe, corresponding to ~150 μM). The combined concentration of these three pools (600 μM) represents ~80% of the total Fe in fermenting mitochondria. This is again a larger-than-expected proportion of mitochondrial Fe in the form of Fe pools. Whether these pools are independent of each other (e.g., imported through different IM transporters) or are in dynamic equilibrium with each other is unknown, but we assume the latter in the model of Figure 7. We have also observed a fourth pool of Fe in fermenting yeast cells, namely mononuclear HS Fe^{III} ions located in a non-mitochondrial region of the cell. The concentration of this pool is high, representing ~75% of all the Fe in the cell.

We have not established the metabolic role of any of these pools. Fe^{II} ions are imported into the mitochondrial matrix via two high-affinity transporters (Mrs3p and Mrs4p), and this pool is used as feedstock for Fe−S cluster and heme biosynthesis. Studies also suggest the presence of an Fe^{III} pool in vacuoles (*23*). It is appealing to consider that we have observed these and perhaps other Fe pools in yeast, but further studies are required to establish this. Mössbauer spectroscopy in combination with the analysis of various genetic strains of yeast will undoubtedly be useful in elucidating this and other details of iron trafficking in cells.

SUPPORTING INFORMATION AVAILABLE

Western blot of isolated mitochondria (Figure S1), Mössbauer spectra of EGTA-washed mitochondria from fermenting cells (Figure S2), effect of sonication (Figure S3), the third and fourth BPS experiments (Figure S4), Western blot of eight independent mitochondrial preparations (Figure S5), effect of deoxycholate on Mössbauer spectra of dithionite-reduced mitochondria (Figure S6), and Mössbauer spectrum of whole fermenting yeast cells after sonication and treatment with dithionite (Figure S7). This material is available free of charge via the Internet at http://pubs.acs.org.

REFERENCES

1. Atamna, H. (2004) Heme, iron, and the mitochondrial decay of ageing. *Ageing Res. Rev. 3*, 303–318.
2. Mühlenhoff, U., Stadler, J. A., Richhardt, N., Seubert, A., Eickhorst, T., Schweyen, R. J., Lill, R., and Wiesenberger, G. (2003) A specific role of the yeast mitochondrial carriers Mrs3/4p in mitochondrial iron acquisition under iron-limiting conditions. *J. Biol. Chem. 278*, 40612–40620.
3. Shvartsman, M., Kikkeri, R., Shanzer, A., and Cabantchik, Z. I. (2007) Non-transferrin-bound iron reaches mitochondria by a chelator-inaccessible mechanism: Biological and clinical implications. *Am. J. Physiol. 293*, C1383–C1394.
4. Lesuisse, E., Santos, R., Matzanke, B. F., Knight, S. A. B., Camadro, J. M., and Dancis, A. (2003) Iron use for haeme synthesis is under control of the yeast frataxin homologue (Yfh1). *Hum. Mol. Genet. 12*, 879–889.
5. Tangeras, A., Flatmark, T., Backstrom, D., and Ehrenberg, A. (1980) Mitochondrial iron not bound in heme and iron-sulfur centers: Estimation, compartmentation and redox state. *Biochim. Biophys. Acta 589*, 162–175.
6. Petrat, F., de Groot, H., Sustmann, R., and Rauen, U. (2002) The chelatable iron pool in living cells: A methodically defined quantity. *Biol. Chem. 383*, 489–502.
7. Petrat, F., Weisheit, D., Lensen, M., de Groot, H., Sustmann, R., and Rauen, U. (2002) Selective determination of mitochondrial chelatable iron in viable cells with a new fluorescent sensor. *Biochem. J. 362*, 137–147.
8. Miao, R., Martinho, M., Morales, J. G., Kim, H., Ellis, E. A., Lill, R., Hendrich, M. P., Munck, E., and Lindahl, P. A. (2008) EPR and Mössbauer spectroscopy of intact mitochondria isolated from yah1p-depleted *Saccharomyces cerevisiae*. *Biochemistry 47*, 9888–9899.
9. Hudder, B. N., Morales, J. G., Stubna, A., Münck, E., Hendrich, M. P., and Lindahl, P. A. (2007) Electron paramagnetic resonance and Mössbauer spectroscopy of intact mitochondria from respiring *Saccharomyces cerevisiae*. *J. Biol. Inorg. Chem. 12*, 1029–1053.
10. Diekert, K., de Kroon, A. I. P. M., Kispal, G., and Lill, R. (2001) Isolation and subfractionation of mitochondria from the yeast *Saccharomyces cerevisiae*. *Methods Cell Biol. 65*, 37–51.
11. Stevens, B. J. (1977) Variation in number and volume of mitochondria in yeast according to growth-conditions: Study based on serial sectioning and computer graphics reconstitution. *Biol. Cell 28*, 37–56.
12. Lindahl, P. A., Morales, J. G., Miao, R., and Holmes-Hampton, G. (2009) Isolation of *Saccharomyces cerevisiae* mitochondria for Mössbauer, EPR, and electronic absorption spectroscopic analyses. In Methods in Enzymology, Ch 15, pp 267−285, Academic Press, New York.
13. Luo, Y., Bond, J. D., and Ingram, V. M. (1997) Compromised mitochondrial function leads to increased cytosolic calcium and to activation of map kinases. *Proc. Natl. Acad. Sci. U.S.A. 94*, 9705–9710.
14. Dickson, D. P. E., and Berry, F. J. (1986) Mössbauer Spectroscopy, Cambridge University Press, Cambridge, U.K.
15. Wikstrom, M., Krab, K., and Saraste, M. (1981) Proton-translocating cytochrome complexes. *Annu. Rev. Biochem. 50*, 623–655.
16. Kent, T. A., Münck, E., Dunham, W. R., Filter, W. F., Findling, K. L., Yoshida, T., and Fee, J. A. (1982) Mössbauer study of a bacterial cytochrome-oxidase: Cytochrome c1aa3 from *Thermus thermophilus*. *J. Biol. Chem. 257*, 2489–2492.
17. Miao, R., Kim, H., Koppolu, U. M. K., Ellis, E. A., Scott, R. A., and Lindahl, P. A. (2009) Biophysical characterization of the iron in mitochondria from Atm1p-depleted *Saccharomyces cerevisiae*. *Biochemistry 48*, 9556–9568.
18. Garber-Morales, J., Holmes-Hampton, G. P., Miao, R., Guo, Y., Münck, E., and Lindahl, P. A. Biophysical Characterization of Iron in Mitochondria Isolated from Respiring and Fermenting Yeast (manuscript in preparation).

19. Flatmark, T., and Tangeras, A. (1976) Mitochondrial 'non-heme non-FeS iron' and its significance in the cellular metabolism of iron. In Proteins of iron metabolism (Brown, E. B., Fielding, J., and Crichton, R. R., Eds.) pp 349−358, Grune & Stratton, New York.
20. Glick, B. S., and Pon, L. A. (1995) Isolation of highly purified mitochondria from *Saccharomyces cerevisiae*. *Methods Enzymol. 260*, 213–223.
21. Goetz, J. G., and Nabi, I. R. (2006) Interaction of the smooth endoplasmic reticulum and mitochondria. *Biochem. Soc. Trans. 34*, 370–373.
22. Green, D. E., Tisdale, H. D., Criddle, R. S., and Bock, R. M. (1961) Structural protein and mitochondrial organization. *Biochem. Biophys. Res. Commun. 5*, 81.
23. Singh, A., Kaur, N., and Kosman, D. J. (2007) The metalloreductase Fre6p in Fe-efflux from the yeast vacuole. *J. Biol. Chem. 282*, 28619–28626.